SANDIA REPORT

SAND2003-3430
Unlimited Release
Printed September 2003

Assessment of the Non-Destructive Nature of PASD on Wire Insulation Integrity

Steven F. Glover, Matthew B. Higgins, Gary E. Pena, Larry Schneider

Prepared by
Sandia National Laboratories
Albuquerque, New Mexico 87185 and Livermore, California 94550

Sandia is a multiprogram laboratory operated by Sandia Corporation,
a Lockheed Martin Company, for the United States Department of Energy's
National Nuclear Security Administration under Contract DE-AC04-94AL85000.

Issued by Sandia National Laboratories, operated for the United States Department of Energy by Sandia Corporation.

Available to DOE and DOE contractors from
U.S. Department of Energy
Office of Scientific and Technical Information
P.O. Box 62
Oak Ridge, TN 37831

Telephone: (865)576-8401
Facsimile: (865)576-5728
E-Mail: reports@adonis.osti.gov
Online ordering: http://www.doe.gov/bridge

Available to the public from
U.S. Department of Commerce
National Technical Information Service
5285 Port Royal Rd
Springfield, VA 22161

Telephone: (800)553-6847
Facsimile: (703)605-6900
E-Mail: orders@ntis.fedworld.gov
Online order: http://www.ntis.gov/help/ordermethods.asp?loc=7-4-0#online

SAND2003-3430
Unlimited Release
Printed September 2003

Assessment of the Non-Destructive Nature of PASD on Wire Insulation Integrity

Steven F. Glover, Matthew B. Higgins, Gary E. Pena, Larry Schneider
Applied Accelerator and EM Technologies Department
and
Thomas R. Lockner
Beam Applications and Initiatives Department
Sandia National Laboratories
P. O. Box 5800
Albuquerque NM 87185-1152

Abstract

The potential of a new cable diagnostic known as Pulse-Arrested Spark Discharge technique (PASD) is being studied. Previous reports have documented the capability of the technique to locate cable failures using a short high voltage pulse[1]. This report will investigate the impact of PASD on the sample under test. In this report, two different energy deposition experiments are discussed. These experiments include the PASD pulse (~6 mJ) and a high energy discharge (~600 mJ) produced from a charged capacitor source. The high energy experiment is used to inflict detectable damage upon the insulators and to make comparisons with the effects of the low energy PASD pulse. Insulator breakdown voltage strength before and after application of the PASD pulse and high energy discharges are compared. Results indicate that the PASD technique does not appear to degrade the breakdown strength of the insulator or to produce visible damage. However, testing of the additional materials, including connector insulators, may be warranted to verify PASDs non-destructive nature across the full spectrum of insulators used in commercial aircraft wiring systems.

Acknowledgements

We are grateful to. Parris Holmes for the construction and operation of the pulser facilities.

Table of Contents

Table of Figures

1 Introduction

As the US commercial airline fleet ages, the need for a variety of reliable system diagnostics will increase. One of the most difficult subsystems to test is the internal wiring. Fatigue or chaffing of control, power, and diagnostic cables can lead to unreliable flow of power and communication signals in addition to coupling to other systems in the aircraft further decreasing reliability. Identification of cable damage needs to be performed before the damage becomes a performance threat. Because of the lengths of the cable runs and their inaccessibility, a diagnostic technique to determine both the presence and location of cable faults would be of great assistance to the industry.

Sandia National Laboratory has developed a diagnostic technique that can fill this requirement under many circumstances. It is based upon the principle that a short pulse of electrical energy can propagate between two conductors over long distances with little loss in energy. If the pulse voltage is large enough, defects in the insulation between the conductors can be located by initiating a breakdown between them. At the breakdown location, some of the pulse energy will be reflected. This energy can be detected at the pulse source and used to determine the breakdown location. In essence, the PASD technique uses a high voltage time domain reflectometer (TDR) technique to locate insulation defects that lower the breakdown strength of the cable.

This report addresses a critical question associated with the technique. Does the diagnostic increase the damage to the cable system? It is important that if a defect is not detected or is within acceptable limits, the diagnostic does not cause additional deterioration. The requirement that the diagnostic not aggravate existing damage is similar to the Hippocratic Oath in medicine which requires that doctors 'first do no harm'.

We have chosen to address this question in three ways. First, we assess the breakdown history over several pulses on the same surface. If the PASD pulse is damaging the surface, we should see a reduction in voltage strength of the surface after the first pulse. Since breakdown is a statistical process, we have performed tests on multiple samples to see if there is a statistically significant change.

Second, if it can be demonstrated that the pulse does not do additional damage under normal test conditions, it is important to know the damage threshold to determine the safety margin of the technique. To this end, we have also performed experiments to identify surface breakdown energy levels at which damage to a typical electrical insulator are detectable. If the result of breakdown tests with large energy deposited in the arc indicates that the damage threshold is significantly above the energy in the PASD pulse, then the argument can be made that even for unusual circumstances, the PASD test will not lead to deterioration in voltage breakdown strength of the cable in question.

Finally, microscopic comparison of insulator samples exposed to the voltage breakdown conditions considered in this report is performed. Photographs of insulator samples taken before and after the voltage breakdown are compared.

This report is organized in the following manner. The next section discusses energy deposition, three methods used to deposit energy across the sample, and the calculations used to determine the energy deposited by each method. These methods are referred to as PASD energy deposition, high energy deposition (higher than PASD), and low energy deposition (lower than PASD). Following the discussion on energy deposition techniques are the description of the experiments used to evaluate the damage and possibility of damage cause by the PASD pulse. The report concludes with statement of the results and suggested future experiments

2 Energy Deposition

Before proceeding to describe the experiments, it is useful to develop a picture of the breakdown energy deposition process. In the process of breaking down an insulator between two conducting surfaces, the resistance goes from a semi-infinite value to a very low value defined by the physical properties of the discharge. The character of the energy deposition in the arc depends on the source impedance of the supply and the pulse length. It is well known[2] that the maximum power transfer occurs when the load impedance is equal to the source impedance. For a pulse length on the order of the breakdown time, the energy deposition will occur as the impedance drops to about the source impedance. For a very long pulse, the energy deposition can be dominated by the low impedance phase of the arc instead of the short period where the impedance is matched to the source.

For the PASD pulse, we have a short pulse (tens of nanoseconds) delivered from a 25 ohm source (50 ohm cable into a 50 ohm cable in parallel with the discharge). As will be shown below, the energy deposition for this case is dominated by the very short period when the arc impedance is ~25 ohms. For the high energy deposition experiments, a capacitor is discharged through the arc. In this case, not only is there a lower impedance source, but the time over which the energy is deposited is long since the pulse is terminated only by the lack of energy in the source. While the energy deposition in the two experiments is in two very different regimes, we make the assumption that damage is due to the total energy deposited as long as the deposition time is short compared with a thermal diffusion time in the material. We assume that during a discharge with sufficient energy deposition, the material properties are altered to reduce the voltage breakdown level in subsequent tests. This might be manifested as the creation of a surface carbon layer left from the breaking of the hydrogen bonds at high temperature.

2.1 PASD energy deposition

To generate the PASD pulse a high voltage pulse source is used. This pulser is similar but not identical to the transmission line pulser used in reference 1 and depicted in Figure 1. The change in pulsers was a result of data acquisition issues described in

section 0. These issues led us to use a blumlein pulser configuration shown in Figure 2. This configuration has the advantage of producing an output pulse that is approximately the same amplitude as the charge voltage (as opposed to the transmission line pulser which generates a pulse ½ the amplitude of the cable charge). The normal drawback of the blumlein pulser is the slower risetime and wider pulse length, as seen in Figure 3. However in this case, the longer risetime is an advantage. In these experiments the insulator breakdown occurs during the risetime of the applied pulse which is on the same timescale as the original PASD pulse. It is assumed that the effects described here are independent of the two pulse shapes since the amplitudes and timescales are comparable.

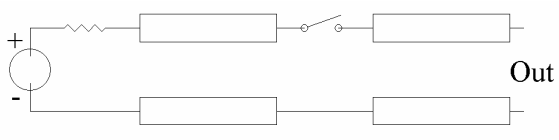

Figure 1. Transmission line pulser

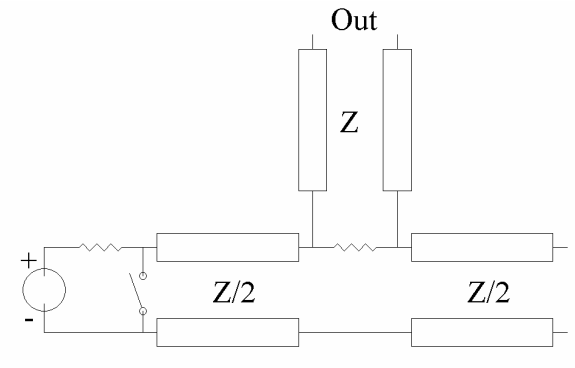

Figure 2. Blumlein pulser

2.1.1 Experimental Setup

The overall layout of the pulse test configuration is shown in Figure 4 and is followed by a photograph of the testbed in Figure 5. The pulse is transmitted through a 20 foot cable to an Edot monitor which measures the incident and reflected pulses. The monitor is isolated from the load by another 20 foot cable to separate the incident from the reflected pulse in time. A second Edot monitors the voltage at the load. The load is connected to a terminated 50 ohm cable where the transmitted pulse is measured using a resistive divider network. During high voltage pulse operation, the resistive monitor is not used but the cable is terminated so that the case for Z_{load}= open circuit produces no reflection. For some experimental configurations where the voltage was not adequate to consistently break down the insulating surface, the 50 ohm cable and termination were removed yielding a voltage doubling at the load.

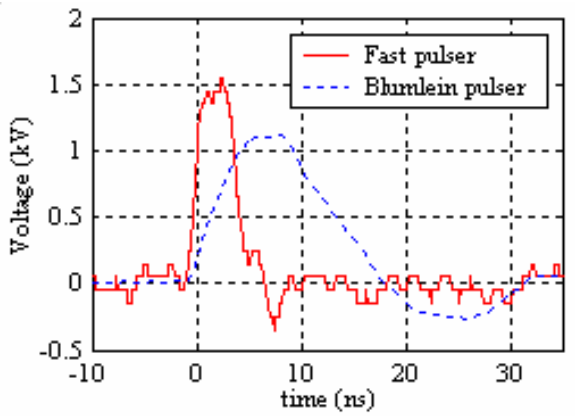

Figure 3. PASD and blumlein pulse comparison.

The second part of the hardware was the arc test fixture which held the insulating breakdown surface. An illustration of this fixture is shown in Figure 6, followed by photographs in Figure 7 and Figure 8. An aluminum block was drilled and tapped to allow insertion of a BNC solder lug connector on one side and a 5/16-20 threaded rod on the other. A collar was screwed into the BNC fitting side with a center hole that

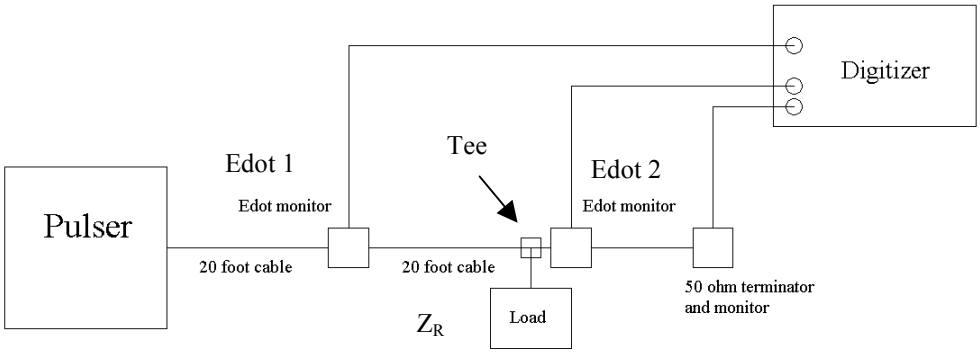

Figure 4. Pulse source test configuration

allowed the center pin of the BNC connector to clear it. The high voltage pulse was applied to the BNC connector and the pulse voltage appeared across the gap between the BNC center pin and the collar. The test insulator was inserted between the collar and the threaded rod and compressed slightly by both the threaded rod and BNC center pin. In this way, there was a consistent mechanical connection between the collar and center pin edges and the test insulator, giving a consistent geometry for the surface breakdown. An insulating spacer was also inserted between the test insulator and threaded rod on some experiments to reduce the field enhancement at the collar and center pin edges.

2.1.2 Edot calibration

Transmission line voltage measurements were made by placing Edot probes at two transmission line locations (Figure 4). The Edot probe was fabricated from a type HN bulkhead feedthrough and UG-250 semi-rigid coax (Figure 9). A hole was milled through the outer conductor of the feedthrough and the the semi-rigid coax was attached so the center

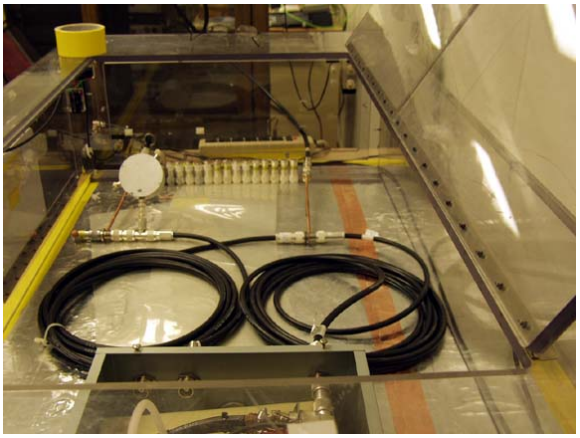

Figure 5. PASD experimental configuration. The PASD pulse generator is at the bottom and the coils of cable are used to isolate the pulser from the

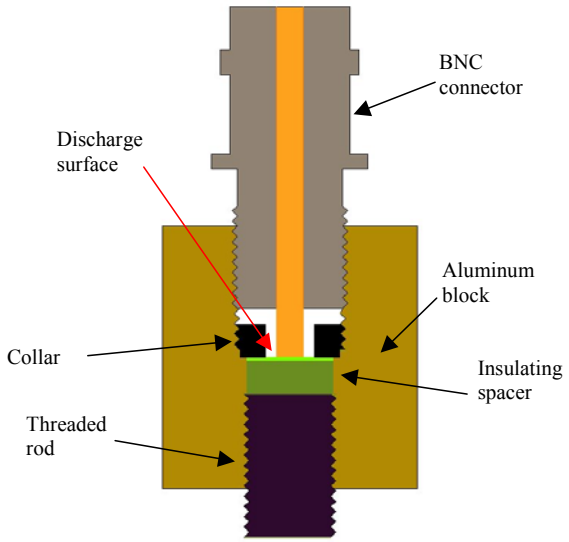

Figure 6. Arc test fixture.

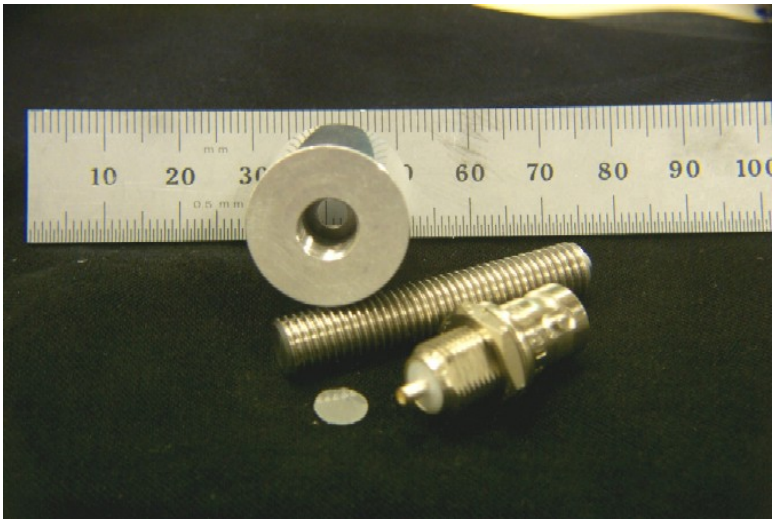

Figure 7. Arc test fixture disassembled.

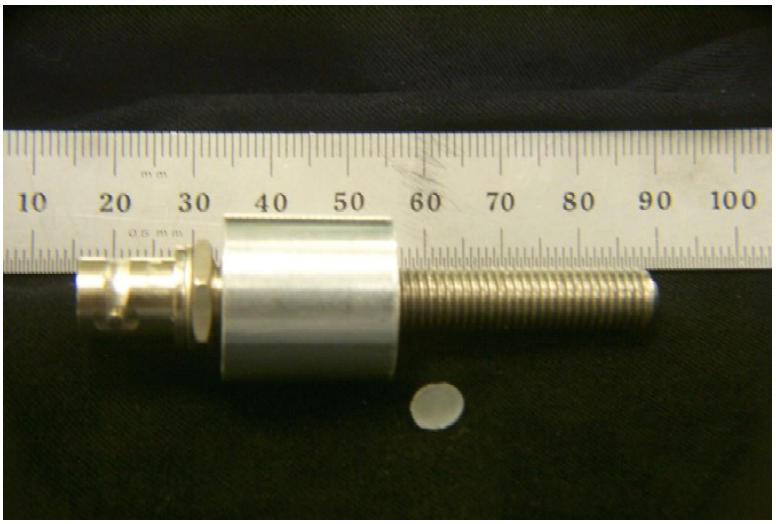

Figure 8. Arc test fixture assembled.

conductor was flush with the outer diameter of the connector insulation. As the pulse propagates past the semi-rigid coax, the electric field from the pulse induces a charge transfer on the coax center conductor. The charge transfer generates a voltage pulse which propagates through the semi-rigid coax to a digitizer where it is recorded. It can be shown that the voltage pulse induced on the semi-rigid coax is proportional to the derivative of the electric field in the bulkhead feedthrough. By integrating this signal, an accurate measure of the main voltage pulse can be acquired.

Calibration of the Edot probes was accomplished by connecting the three probes together with male-to-male HN connectors and inserting this assembly between the pulser and resistive voltage monitor. The Edots were isolated from the pulser and monitor by 10 feed of coaxial cable. The signal recorded from the resistive monitor gave us a direct measurement of the pulse monitored by the Edots. Edot 1 and Edot 2

probe signals were recoded on Tektronix TDS744A and TDS684A digitizers, soft integrated, baselined, and compared to the directly measured signal to calculate a gauge factor for that probe.

In order to measure the total pulse energy, a high fidelity voltage measurement was necessary. In our initial experiments, a transmission line pulser (Figure 1) was used, which produced a 7 ns pulse with a 1.25 ns risetime. The derivative of this signal (generated by the Edots) was only as wide as the pulse rise and fall times. Because this signal must be software integrated (signal levels were too low for hard integration), a high fidelity measurement needed a 10 Ghz sampling rate. The limitations of our 2 GHz (TDS744A) and 5 GHz (TDS684A) sampling rates were made apparent from initial calibration attempts and the first experimental measurements. The calibration signals looked as though they had passed through a low pass filter, and the initial experimental measurements indicated a much larger amplitude variation than the resistive monitor. Sampling only 2 points during the pulse risetime lead to large variations in integrated pulse height depending on where the samples happened to land. This problem was solved by using the Blumlein pulser (Figure 2) with its slower risetime. By sampling 10 points during the risetime, the variations in pulse energy from sampling errors were reduced significantly.

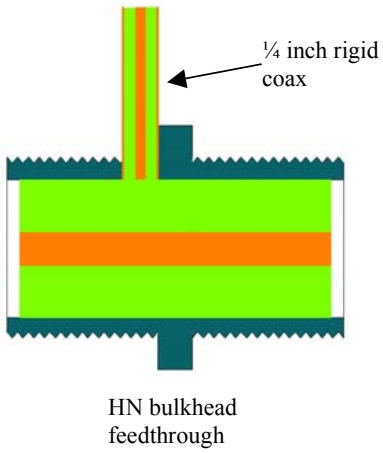

Figure 9. Edot monitor configuration. Insulators are shown in green and conductors in orange or grey.

During the calibration measurements, the probes were placed in various configurations to investigate any effects the presence of the probes had on the signal in the transmission line. It was found that there was no measurable perturbation due to the presence of the probes.

2.1.3 Resistive Validation

Before any attempt was made to measure the energy deposited in a discharge, a set of resistive measurements were made to determine the sensitivity of the entire system and validate the measurement technique. A fixed carbon composite resistor in a low inductance configuration was placed at the load position shown in Figure 4. The load resistance was varied and the signals were measured on the first and second Edot probes. The values for the measured load resistance were: 10.7, 15.6, 18.4, 28.2, 33.7, 50.5, 51.2, 102.6, 151.1, 243.1, 514, 703, 843, and 1228 ohms. The experimental results were compared with calculations of the expected energy absorption to determine the accuracy of the system.

First we present a brief derivation of the equation used in determining the theoretical values of energy absorption due to a parallel resistance[3]. For the theoretical equation derivations, we are looking for the power absorbed by the load resistor (P_{toR}) and the power delivered to the end termination resistor (P_{toEND}).

The parallel impedance of the Tee is given by

$$Z_{Tee} = \frac{Z_o Z_R}{Z_o + Z_R}, \tag{1}$$

where Z_0 is the transmission line impedance and Z_R is the load impedance. The voltage reflection coefficient is given by

$$\Gamma_{Tee} = \frac{Z_{Tee} - Z_o}{Z_{Tee} + Z_o}. \tag{2}$$

By squaring equation (2), the power reflection coefficient at the Tee is

$$\Gamma_{PTee} = \Gamma_{Tee}^2 \tag{3}$$

and whatever is not reflected is transmitted, so the power transmission coefficient at the Tee is

$$T_{PTee} = 1 - \Gamma_{PTee}. \tag{4}$$

Therefore, the power delivered to the load on the Tee is found by multiplying the power transmission coefficient by the load branch of the voltage divider circuit resulting in

$$P_{toR} = T_{PTee}\left(\frac{\frac{1}{Z_R}}{\frac{1}{Z_R} + \frac{1}{Z_o}}\right). \tag{5}$$

The rest of the power transmitted must go to the termination at the end of the experimental setup, which is calculated by

$$P_{toEND} = T_{PTee}\left(\frac{\frac{1}{Z_o}}{\frac{1}{Z_o} + \frac{1}{Z_R}}\right). \tag{6}$$

For the experiment, the fraction of total input pulse energy that was absorbed by the load was calculated by subtracting the transmitted and reflected pulse energy from the energy of the incoming pulse. Edot 1 was separated to yield the input and reflected

pulse, and Edot 2 used for the transmitted pulse. The signals were baselined, integrated, squared, and divided by 50 (transmission line impedance) to yield the power pulse. This signal was then integrated again to obtain the total pulse energy.

Figure 10 shows the theoretical and measured energy absorbed as the load resistance is varied. The experimental data is in good agreement with the theory over a wide range of impedances. There is less that a 5% difference in the average measured energy absorbed compared to the theoretical values. This demonstrates the capability of the system to measure energy deposition over a wide range as is necessary for the arc measurements. The difference between the experimental measurements and calculations at high impedance is due to the electrical noise in the system. This has a small effect on the arc measurements.

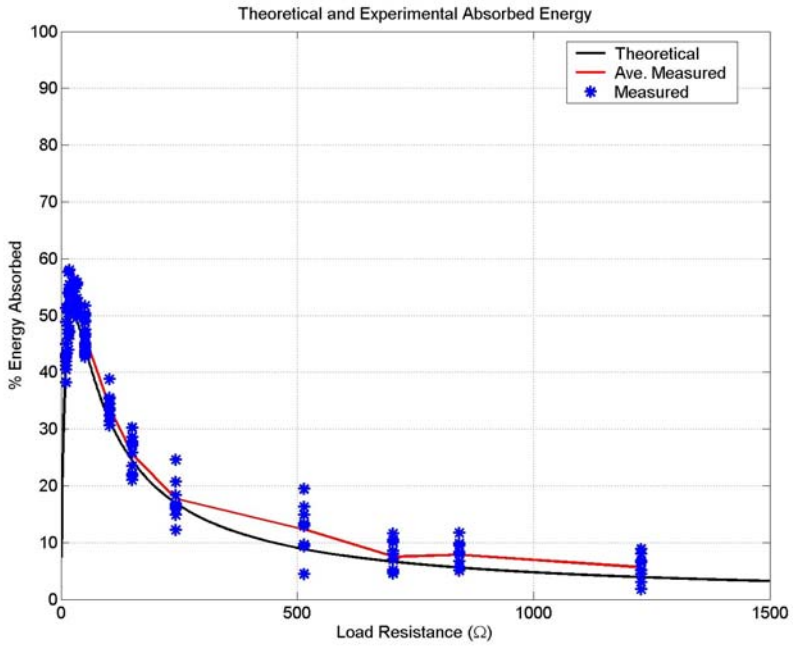

Figure 10. Plots of experimentally measured and calculated energy absorbed for known load resistances.

2.2 High Energy Deposition

While the previous section describes the PASD pulse testbed and defines the technique for estimating the energy deposited by the pulse comparisons will also be made to higher energy breakdowns. To develop the means for making these comparisons a separate testbed was constructed. This section describes this testbed along with the calculations used to determine the circuit parameters and the arc energy of the high energy breakdowns.

2.2.1 Experimental setup

A schematic of the experiment is shown in Figure 11. The testbed includes a Glassman high voltage power supply connected through a 10MΩ charging resistor and a high voltage relay (S1) to 177nF of energy storage capacitance. The capacitance is connected in parallel with the arc test fixture/sample through the high voltage relay (S2). A photograph of the testbed not including the power supply is shown in Figure 12. The procedure for performing this experiment is:

1. close S1 and open S2
2. charge the capacitor to a voltage greater than the expected breakdown voltage
3. open S1
4. close S2

This method allows the energy available to the arc to be varied independent of the capacitance and fixture.

2.2.2 Circuit Parameter Estimation

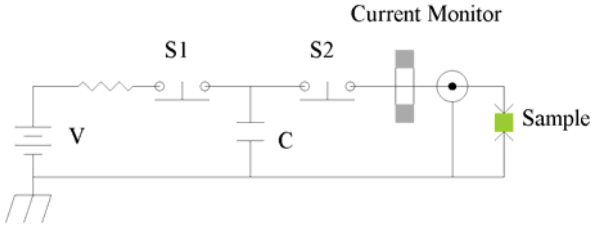

Figure 11. Schematic of high energy discharge experiment.

Figure 12. Large energy deposition experimental layout. Energy storage capacitors are white objects in center, current monitors are shown below.

While relay S1 is open and relay S2 is closed the circuit in Figure 11 can be approximated by a series RLC circuit, as depicted in Figure 13. In Figure 13, C and L represent the energy storage capacitance and the distributed inductance from the circuit and internal to the capacitor. The resistance R_c represents the internal resistance of the capacitor, the circuit contact resistances, and the circuit wire resistances. The resistance R_s represents the arc resistance across the sample. To simplify the analysis the total resistance of the circuit is written as

$$R = R_c + R_s . \qquad (7)$$

The parameters of the circuit in Figure 13 can be estimated from the measured current if the capacitance is known. To begin the derivation of the necessary equations, the circuit parameters must first be defined in terms of characteristics

of the measured current. The differential equation describing the current flow in this circuit is

$$i'' + \frac{R}{L} i' + \frac{1}{LC} i = 0 , \qquad (8)$$

where

$$i' = \frac{di}{dt} . \qquad (9)$$

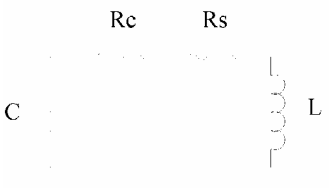

Figure 13. RLC equivalent circuit of the high energy discharge experiment.

The solution to equation (8) may be written as

$$i(t) = i_{pk} e^{-\delta t} (\cos(\varpi t) + \sin(\varpi t)) \qquad (10)$$

where the damping coefficient is

$$\delta = \frac{R}{2L} , \qquad (11)$$

the frequency of oscillation is

$$\omega = \sqrt{\frac{1}{LC} - \delta^2} \text{ radians per second,} \qquad (12)$$

and i_{pk} is the peak value of the undamped current ($\delta = 0$) in amps. The capacitance C is measured directly prior to the experiment and the constants, i_{pk}, δ, and ω are determined indirectly from the current measured during the experiment. Therefore, assuming that the constants C, i_{pk}, δ, and ω are known the circuit inductance is derived from equation (12) and written as

$$L = \frac{1}{C(\omega^2 + \delta^2)} . \qquad (13)$$

Similarly the resistance in the circuit is determined by rearranging equation (11) to get

$$R = 2\delta L . \qquad (14)$$

Now that L and R are defined in terms of measurable quantities the following four steps define the process for extracting the constants i_{pk}, δ, and ω from the measured current data.

1. Remove the DC offsets from the data. First determine the average DC value of the current (DC_{avg}) in the regions for which it should be zero, as indicated in Figure 14. Then adjust the current by:

$$i(n) = i(n) - DC_{avg} \text{ for } n = 1 \ldots N_{samp} \tag{15}$$

where N_{samp} is the total number of data samples.

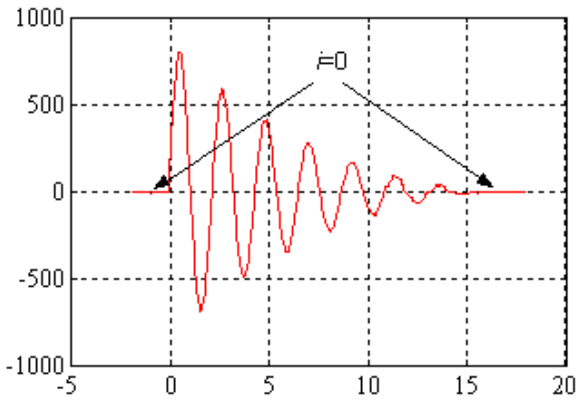

Figure 14. Regions in which the measured current should be zero.

2. Estimate the frequency of Oscillation. First determine a total of N_x zero crossing points from the measured data, as depicted in Figure 15. The frequency of oscillation is then determined from

$$\omega = 2\pi \frac{\sum_{n=1}^{N_x - 1} \frac{1}{2(T_{xn+1} - T_{xn})}}{N_x - 1} \tag{16}$$

where T_{xn} is the time of the nth zero crossing.

3. Shift the measured data in time so that the measured and approximated currents align in time, as depicted in Figure 16. This is accomplished by calculating the time at which the approximated current first crosses zero for $t > 0$ as

$$T_{xa} = \frac{\pi}{\varpi} \tag{17}$$

and estimating the first negative going crossing of the measured data (T_{xm}). Then the time associated with each measured current sample is adjusted by

$$t(n) = t(n) + T_{xa} - T_{xm} \text{ for } n = 1 \ldots N_{samp}. \quad (18)$$

This allows equation (10) to be simplified to

$$i(t) = i_{pk} e^{-\delta t} \sin(\varpi t) \quad (19)$$

by forcing the measured current to be a damped sine wave with zero phase shift for $t >= 0$.

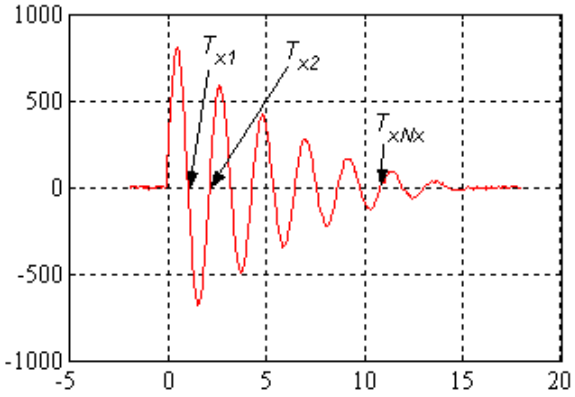

Figure 15. Measured current zero crossings.

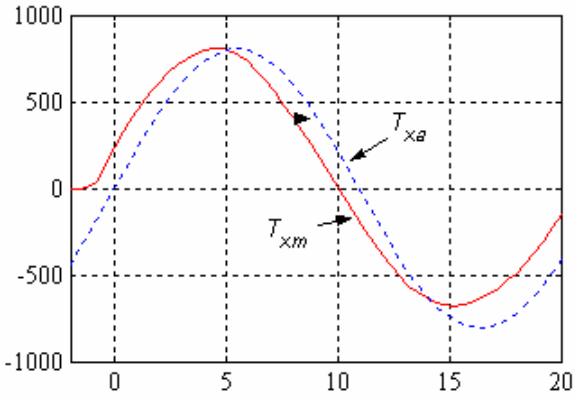

Figure 16. Measured current phase shift correction.

4. The damping coefficient is determined next. First take the absolute value of the measured current as shown in Figure 17. Then determine the peak value of the current (I_{pk}) from N_{pk} half cycles along with the time at which the peaks occur (T_{pk}). The damping ratio is then calculated by

$$\delta = \frac{\sum_{n=1}^{N_{pk}-1}\left(\frac{1}{T_{pkn}-T_{pkn+1}}\right)\ln\left(\frac{I_{pkn+1}}{I_{pkn}}\right)}{N_{pk}-1} \tag{20}$$

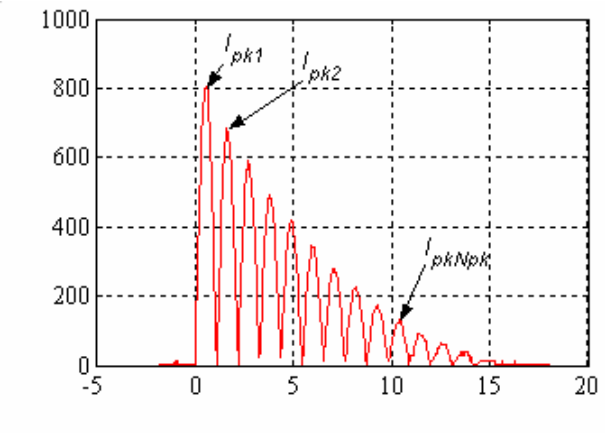

Figure 17. Absolute value of the measured current.

5. The last step in approximating the measured current is determining the peak value of the undamped current (i_{pk}). This is not necessary in order to determine the circuit parameters but does allow for the approximated current to be compared to the measured current as shown in Figure 18. The peak value of the undamped current is calculated by

$$i_{pk} = \frac{\sum_{n=1}^{N_{pk}} \frac{I_{pkn}}{e^{-dT_{pkn}}}}{N_{pk}}. \tag{21}$$

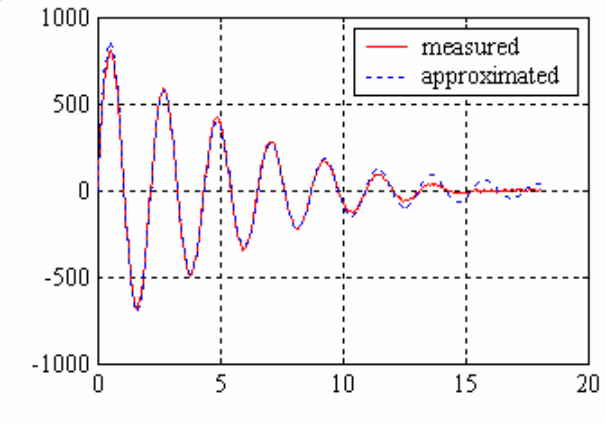

Figure 18. Measured and approximated currents.

2.2.3 Arc Energy Calculation

To estimate the energy dissipated in the arc for high energy deposition, two experiments were performed. The first experiment contained a sample of mylar insulator in the test fixture. From this experiment the total circuit resistance R, as defined in equation 8, is determined. The second experiment has the sample removed and the test fixture shorted, effectively shorting out the resistance R_s. From this experiment the resistance R_c, as depicted in Figure 13, is determined. From these two resistances the sample resistance (R_s) is calculated by

$$R_s = R - R_c . \tag{22}$$

From the sample resistance and measured current the energy deposited in the arc of the first experiment is calculated by

$$E = \sum_{n=1}^{N_{samp}} i^2(n) R_s \Delta t , \tag{23}$$

where $i(n)$ is the nth digitizer sample of the measured current, N_{samp} is the number of samples, and Δt is the time between samples.

Figure 19 and Figure 20 contain plots of the estimated circuit parameters from twelve different experiments. Nine of the experiments used a new sample of mylar insulator with a 3 mil thickness and three of the experiments left the sample insulator out of the test fixture allowing it to short internally. Experiments were performed near three different voltage levels in order to detect arc resistance variation with voltage. The capacitance was measured to be 177 nF. The calculated inductances shown in Figure 19 did not vary with voltage and did not change when using the shorted test fixture. The average value of the inductance is 682.3 nH with a maximum deviation of 2.6%. The circuit resistance during the short circuit test varied little with voltage and had an average resistance of 0.236 Ω, as seen in Figure 20. The circuit resistance with the mylar sample tended to decrease with increasing charge voltage, which is an indication of the changing arc impedance.

Using the resistances plotted in Figure 20 and the measured currents the sample resistances and energies dissipated, during breakdown, are calculated resulting in the values plotted in Figure 21 and Figure 22. Consistent with the results in Figure 20 the arc/sample resistance decreases with increasing charge voltage. This would seem to indicate that at greater charge voltages it should be more difficult to deliver energy to the arc, which is contradicted by Figure 22. However, what maybe happening is that for larger charge voltages the arc remains in a low impedance state for longer periods of time resulting in a lower estimated resistance.

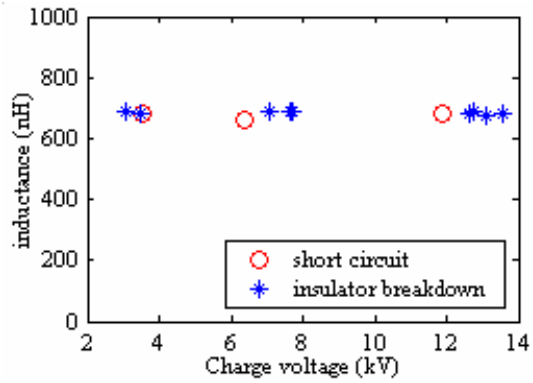

Figure 19. Estimated inductance versus capacitor charge voltage.

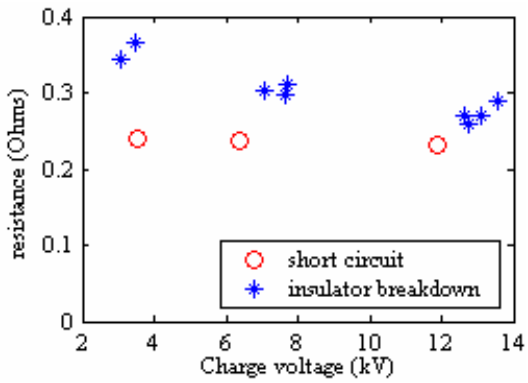

Figure 20. Estimated resistance versus capacitor charge voltage.

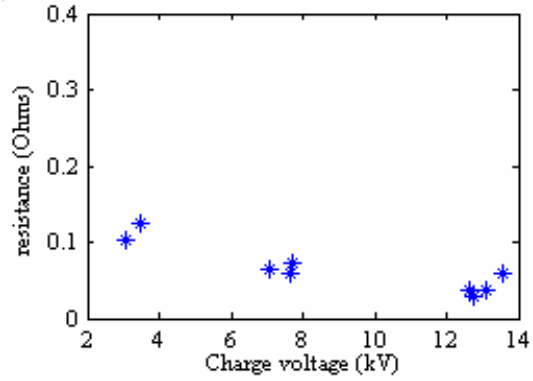

Figure 21. Estimated arc resistance versus capacitor charge voltage.

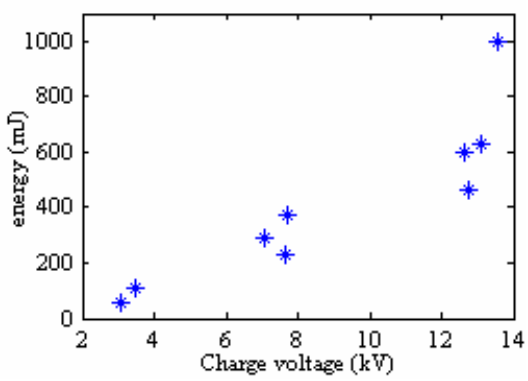

Figure 22. Estimated energy deposition versus capacitor charge voltage.

2.3 Low Energy Deposition

In order to investigate the effects of the PASD pulse and high energy discharge described in the previous sections a lower energy discharge circuit was developed. In the following sections, low energy deposition experiments are defined as voltage breakdown experiments that dissipate energy in the arc at levels significantly lower than the PASD and high energy experiments.

2.3.1 Low Energy Voltage Breakdown

Figure 23 contains the schematic of the experimental setup for the low energy experiments. The differences between this experiment and the high energy experiment are the removal of the energy storage capacitance and the effective removal of the high

voltage relays (the relays were left closed) as can be seen by comparing Figure 11 and Figure 23. For this experiment the voltage level of the power supply is manually slowly increased until voltage breakdown occurs across the sample.

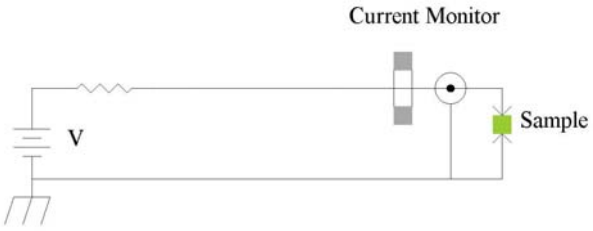

Figure 23. Schematic of low energy discharge experiment.

To demonstrate that the energy deposited in this configuration is well below the PASD energy deposition the energy calculations in this section place an upper bound to the amount of energy that can be deposited during the low energy voltage breakdown. To bound the energy deposited across the sample during low voltage breakdown one must first determine the primary sources of energy available. The first is the power supply which can deliver energy through the 10 MΩ charge resistor. For the sake of bounding the energy delivered to the arc from the power supply the assumptions:

1. the output voltage of the power supply is perfectly regulated
2. the output impedance of the power supply is zero
3. the arc impedance is zero

are made in order to calculate the current delivered from the power supply. The actual current delivered by the power supply will be less than the estimated current due to internal impedances and limited bandwidth of the power supply and the nonzero impedance of the arc. The estimated energy delivered to the arc by the power supply using the maximum possible current is

$$E_{ps} = \left(\frac{v_{dc}}{10^6} \right)^2 R_s \Delta t \,, \tag{24}$$

where v_{dc} is the power supply voltage and Δt is the length of time in which the arc current exists.

The second source of energy to be dissipated in the arc is the energy stored by the parasitic capacitances of the circuit. The parasitic capacitance was measured by disconnecting the power supply and the test fixture from the circuit. Then a capacitance meter was connected to the circuit at the sample end resulting in a measured parasitic capacitance value of $C_p = 50\,pF$. This results in a parasitic energy estimate of

$$E_p = \frac{1}{2} C_p v_{dc}^2 \,. \tag{25}$$

In order to bound the energy delivered to the arc by parasitic energy storage it is assumed that all of the energy in the parasitic capacitance is dissipated by the arc.

The sum E_{ps} and E_p, from equations (24) and (25) respectively, represents an upper bound to the amount of energy that can be dissipated by the arc. From this bound an upper bound can be placed on the ratio of the arc energy dissipated in the low energy voltage breakdown, $E_{ps} + E_p$, to the arc energy dissipated during the PASD pulse, E_{PASD}. This ratio is designated by α_E and defined as

$$\alpha_E = \frac{E_{ps} + E_p}{E_{PASD}}. \tag{26}$$

Table 1. These parameters are based on measurements and results of experiments in this report. Note that for the values of R_s expected in a discharge ($R_s < 100\Omega$) the energy dissipated in the low energy experiment is at least an order of magnitude less than the energy dissipated during the PASD pulse indicating that this is a low energy experiment.

Table 1. Measured and estimated parameters for the low energy calculations.

Parameter	Value
E_{PASD}	5mJ
Δt	15μs
v_{dc}	3kV
C_p	50pF

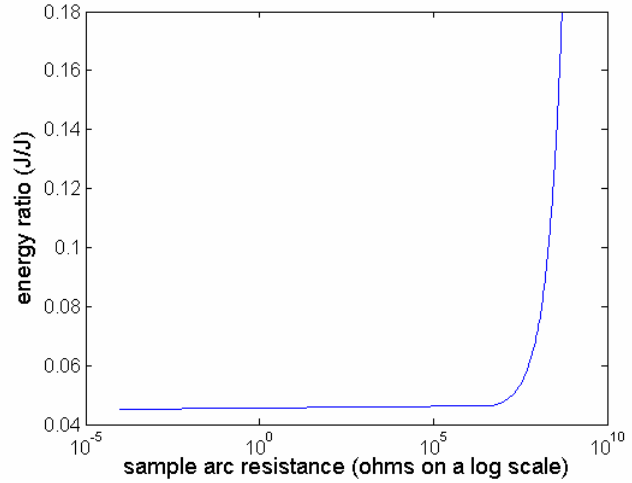

Figure 24. Ratio of the low energy discharge arc energy to the PASD pulse arc energy versus arc resistance.

Now that the energy dissipation level of the low energy experiments is bounded the effects of the PASD and high energy discharges upon the breakdown voltage can be investigated.

3 Experiments

3.1 Breakdown voltage variation over multiple PASD pulses

To determine if there is any indication of insulator degradation and to investigate the energy deposition dependency upon material type four different insulating materials

were tested with the PASD pulser. For each material, 10 new samples were used and a series of 20 pulses were applied to each. We looked for either a drop in breakdown voltage after the first pulse applied to the sample, or a continuous degradation in the breakdown strength as the number of pulses applied to the insulator increased. Each of the set of materials, listed in Table 2, were tested in the 4 different geometrical configurations, listed in Table 3.

Table 2. Insulator materials and their thickness.

	Thickness
Celluloid	0.003-0.005 inches nominal
Mylar	0.003 inches
Teflon	0.03 inches
Polypropolyene	0.06 inches

Table 3. Geometrical configurations

Configuration	Spacer (inches)	Gap (inches)
A	0.0	0.07
B	0.0	0.139
C	0.205	0.07
D	0.205	0.139

Figure 25 shows expanded views of the discharge geometry with and without the insulating spacer. A surface discharge begins when the local electric field is large enough to cause local ionization in the material. The ionization will occur when an electron gains enough energy between collisions to ionize the surrounding medium. For the case of interest, the area of breakdown will be the air at the triple point (air, dielectric, conductor interface). It will occur in the air because this has the longest electron mean free path, and at the triple point because this will be the area of highest electric field. When the electric field meets the above criterion, an electron avalanche begins and usually develops into a streamer and arc as the plasma temperature increases. The arc will develop along the dielectric surface because this is where the largest electric field enhancement occurs as the avalanche moves between the terminals.

The two geometries shown in Figure 25 differ in the size of the electric field at the triple point for a given applied voltage. The electric field on the center pin will be

smaller for the case on the left where the gap between the center pin and ground from the stud is large. On the right, the electric field on the edge of the center pin will be enhanced due to the close proximity of the grounded stud. The effect of the additional field enhancement was seen in the experiments, where the breakdown voltage was sometimes 50% higher with the insulating spacer than without it.

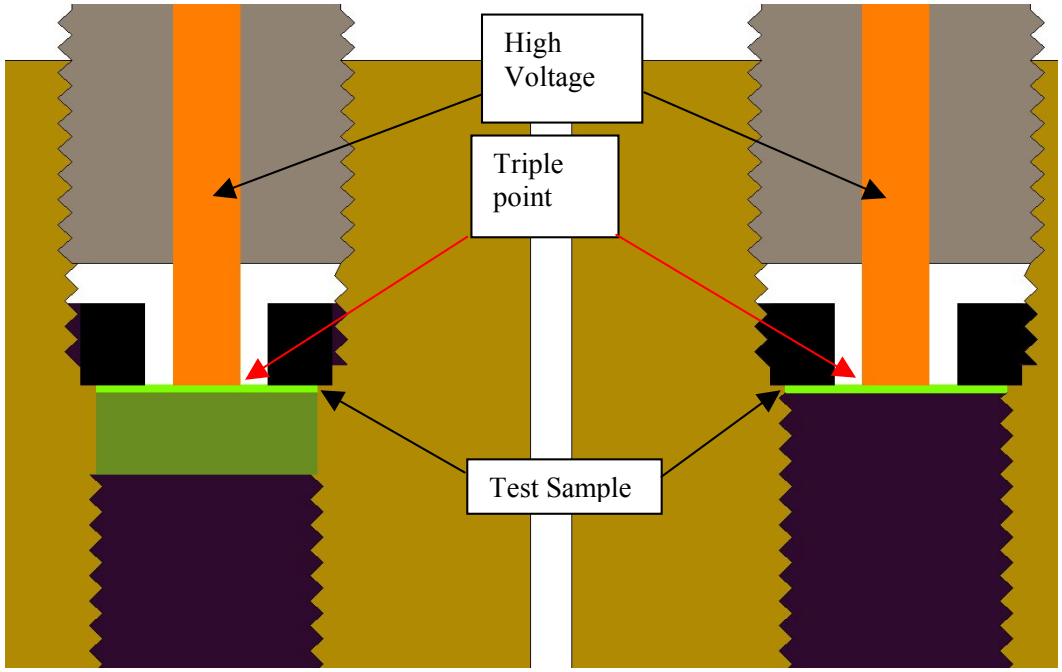

Figure 25. Insulator breakdown test fixture with (left) and without (right) insulating spacer (dark green). Note that with the spacer the field enhancement at the edge of the collar and center pin will be reduced.

Each test sample was punched from a sheet of the material and installed in the test fixture. The pulser was then fired 20 times and the results of each shot were recorded. The average peak pulse voltage was 8456 volts. While there was some variation in this voltage, we do not believe it substantially affected the results presented below.

A typical set of analyzed signals from the two Edot probes is shown in Figure 26. The Edot signals have been baselined and integrated to yield the transmitted, reflected, and incident voltage pulses. Note that the sign has been changed, we will use positive voltage pulses for all analysis. Also shown in Figure 26 is the power into the discharge (green).

Figure 26 illustrates typical breakdown behavior. The transmitted and input voltage rise together while the insulator at the Tee is an open circuit. As the arc forms, the impedance and transmitted voltage drop. At the same time the reflected voltage rises because of the mismatch in impedance as the arc forms. In these traces, the transmitted and reflected pulses have been time shifted from their recorded values to indicate the signal values at the Tee. The arc impedance history calculated from this data is shown

in Figure 27. Note that peak power deposited into the discharge is from ~7-10 ns when the arc impedance ranges from 35 to 10 ohms. This is in agreement with the data of Figure 10. It should also be noted that there is an inductive component to the arc impedance that increases the total somewhat. One result of the inductance is a slight negative overshoot late in the transmitted voltage pulse. While this will influence the voltage and power pulses, the total pulse energy will not be affected.

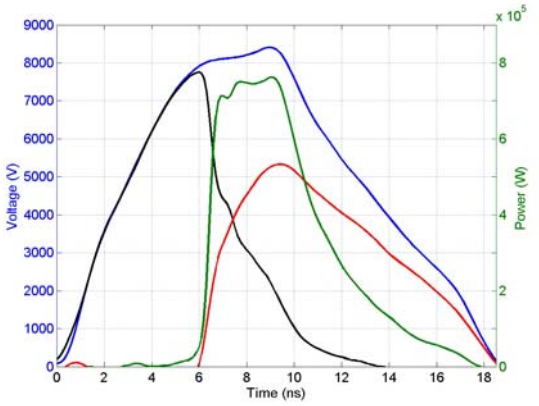

Figure 26. Input (blue), transmitted (black), and reflected voltage (red) pulses. Also shown is the power pulse into the arc (green).

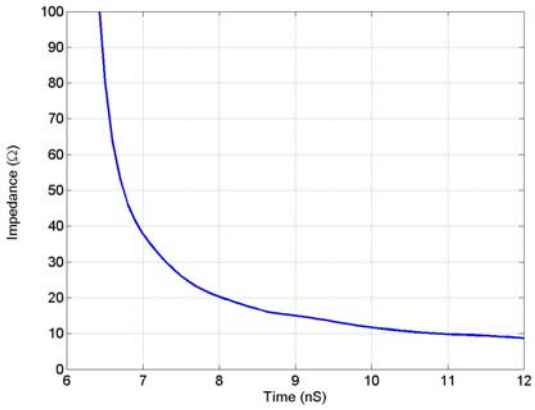

Figure 27. Arc impedance history

For the total energy data shown below, the recorded voltage pulses are used to determine the energy in each pulse from

$$E = \int P(t)dt = \int \frac{V^2}{50} dt \qquad (27)$$

where P(t) is the instantaneous power in the pulse on a 50 ohm cable. From Figure 26, the power pulse is ~4 ns wide and corresponds to the time when the arc impedance is the best match to the cable impedance.

Results for a typical 20 shot run are shown in

Figure 28. In this figure, the breakdown voltage and energy deposited into the discharge are plotted versus shot number. Note that there is no significant change in breakdown voltage after the first shot, and no trend towards lower voltage as the shot series progresses. This is a clear indication that no damage is occurring to the insulator surface under test.

In order to express this type of behavior in a more succinct form for the remainder of the tests, we will define several parameters relevant to the problem.

The development of an arc is a statistical process, leading to significant variations in breakdown voltage from shot to shot. The variation of the breakdown of the first shot relative to the remainder is parameterized by the following

$$< \Delta V >=< (V_n - < V_1 >) > \qquad (28)$$

where $<V_1>$ is the average of the first shot breakdown voltages and V_n is the breakdown voltage of the n^{th} shot. The average on the right is taken over the remaining shots in the run and the standard deviation (σ) is taken over all but the first shot. If there is a drop in the breakdown strength after the first shot, <ΔV> will be negative. If <ΔV>/ σ is larger than 1, then one can attach some statistical significance to the outcome (unless there are other experimental factors to consider).

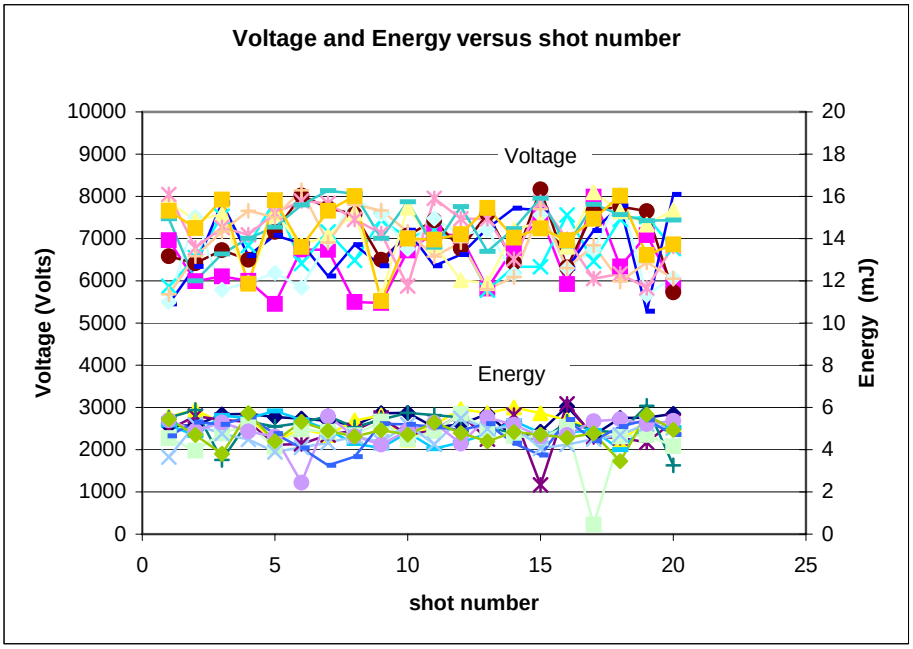

Figure 28. Breakdown voltage and deposited energy versus shot number

Table 4 contains the data describing the breakdown voltage variation from the first pulse, plus a listing of the number of shots in the 20 that did not breakdown and the number that broke down after the peak voltage. Because of the automated routine used to analyze the data, those shots that broke down after the peak voltage were not included in the analysis. The shots that did not break down at all were also excluded. These exclusions in some cases led to a large enough reduction in the number of shots that the statistical significance of the data may not be valid.

Table 4. PASD pulse voltage breakdown results.

No Spacer, Small Gap (A)	<V1>	<ΔV>	<ΔV/σ>	Maximum Absorbed Energy (mJ)	Aver. Absorbed Energy (mJ)	σ of Energy Absorbed	# of no Breakdowns	# of Breakdowns after Peak
Celluloid	4383	-15	-0.16	3.45	2.48	0.40	0	0
Mylar	4423	62	0.63	6.09	5.02	0.41	0	0
Teflon	6217	638	0.87	5.88	4.50	0.65	6	6
Polypropylene	6689	882	1.27	6.02	3.80	0.93	55	43
No Spacer, Large Gap (B)								
Celluloid	6529	-5	-0.06	6.25	5.06	0.39	0	0
Mylar	6732	-13	-0.19	5.87	5.11	0.32	0	0
Teflon	7611	-10	0.09	5.52	4.17	0.74	17	19
Polypropylene	7812	173	11.69	4.93	3.15	0.88	102	42
Spacer, small Gap (C)								
Celluloid	6808	467	0.66	6.31	4.23	0.80	3	2
Mylar	6710	253	0.37	6.17	4.93	0.58	1	1
Teflon	6240	510	0.97	6.25	4.97	0.53	0	3
Polypropylene	6210	1132	1.68	6.38	4.45	1.00	20	19
Spacer, Large Gap(D)								
Celluloid	7882	61	0.31	5.61	3.47	1.11	79	48
Mylar	7516	239	0.97	5.41	4.05	0.82	21	20
Teflon	7829	147	0.44	5.41	3.25	1.10	91	58
Polypropylene	7722	252	1.08	5.45	3.40	1.05	69	46

The results shown in column 2 (<ΔV>) indicate that only 4 of the 16 cases showed a decrease in the average voltage after the first shot, and for those that were negative, the change was well within the statistical variation after the first shot. This is clear evidence that there was no drop in voltage after the first shot, and in a few cases there was actually a significant increase (this could be due to cleaning of the surface by the discharge). The variation in breakdown voltage was in good agreement with the expected behavior. Note that the change in breakdown voltage with and without the spacer was small for the polypropylene since the thickness of the sample was already comparable to the spacer thickness.

The maximum energy absorbed was fairly consistent, ranging from 6.31 to 3.45 mJ for the celluloid with all other materials falling between these values. There appears to be little correlation between breakdown voltage and energy deposition (other than the small gap, no spacer celluloid run). This is somewhat surprising since the energy available varies.

It was observed that the timing of the breakdown changed the energy deposition. Figure 29 shows the variation in energy deposition versus voltage breakdown for the 200 shots fired in configuration C using polypropylene. There is a significant drop in the deposited energy as the breakdown approaches the peak pulser voltage. This is not due to the breakdown voltage directly, but the timing of the arc in the input pulse. For breakdown near the peak voltage, the input pulse is falling during the surface breakdown. This drops the available input power during breakdown and ultimately the total power delivered to the arc. A similar effect would be observed if the pulse length were shortened. This would also lead to a drop in the deposited energy, but could lead to reduced reliability since the number of shots without a breakdown would increase (as seen from the no breakdown data).

3.2 Effect of PASD on low energy Voltage Breakdown

The previous section investigated the effect of multiple PASD pulses upon the breakdown strength of the insulators. This section investigates the effect of a single PASD pulse upon the low energy breakdown voltage of an insulator. For these tests a single material is used, mylar with a 3mil thickness. To investigate the effect of PASD pulse upon the voltage breakdown of the mylar samples the following process is followed.

1. Insert a new insulator sample into the arc test fixture.

2. Initiate low energy breakdown using slowly rising voltage. Repeat 20 times to establish statistical average.

3. Conduct 1 PASD pulse experiment upon the sample using an 8kV pulse.

4. Initiate low energy breakdown using slowly rising voltage. Repeat 20 times to establish statistical average.

Due to the sometimes erratic behavior of the voltage breakdown process some of the measured voltage waveforms had unusual shapes, as can be seen in Figure 30. For this reason the average of the voltage waveforms before any fluctuations began was taken as the breakdown voltage.

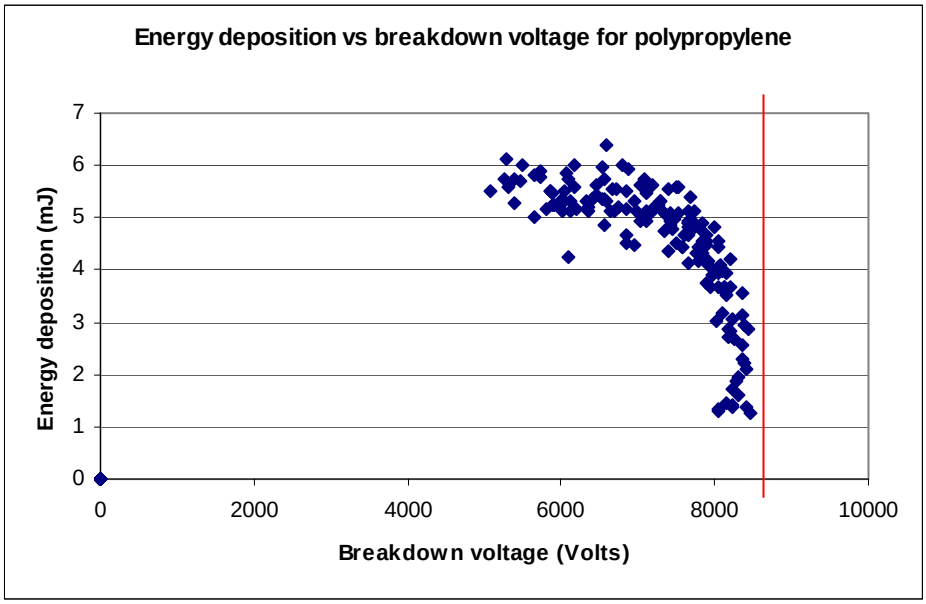

Figure 29. Energy deposition versus breakdown voltage for polypropylene. Note the drop near the peak pulser voltage (red line).

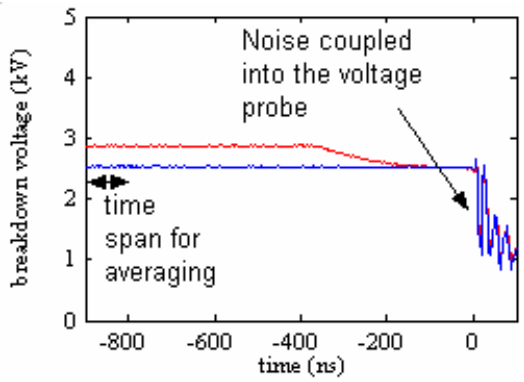

Figure 30. Example of measured voltages during two different low energy breakdown experiments.

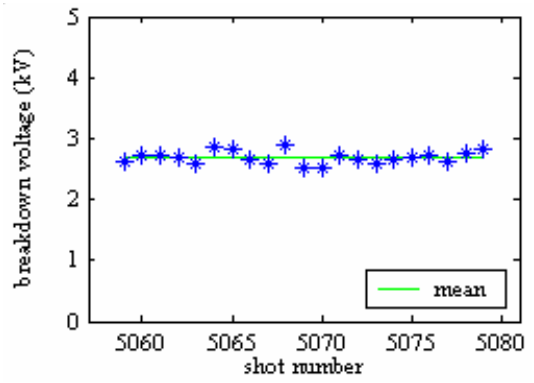

Figure 31. Low energy voltage breakdown test 1 results before a PASD shot.

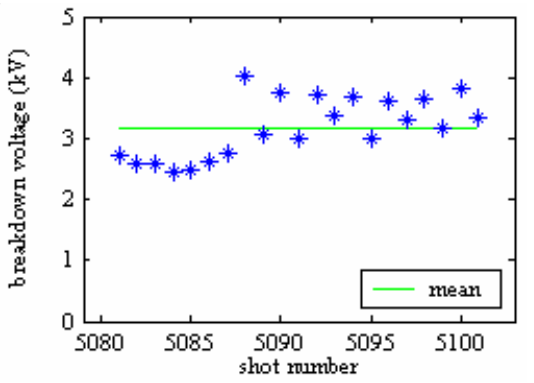

Figure 32. Low energy voltage breakdown test 1 results after a PASD shot.

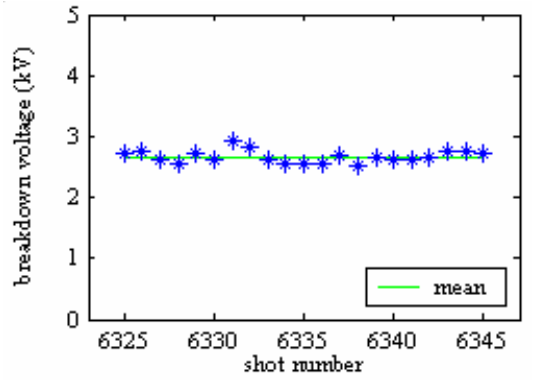

Figure 33. Low energy voltage breakdown test 2 results before a PASD shot.

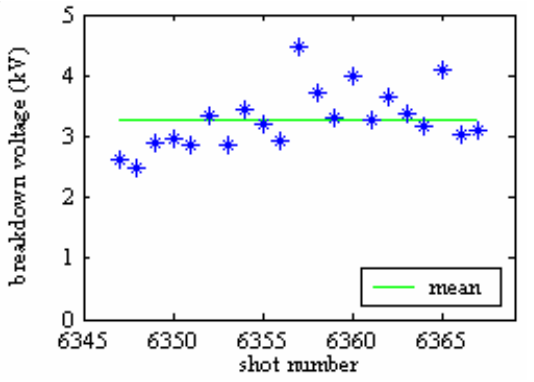

Figure 34. Low energy voltage breakdown test 2 results after a PASD shot.

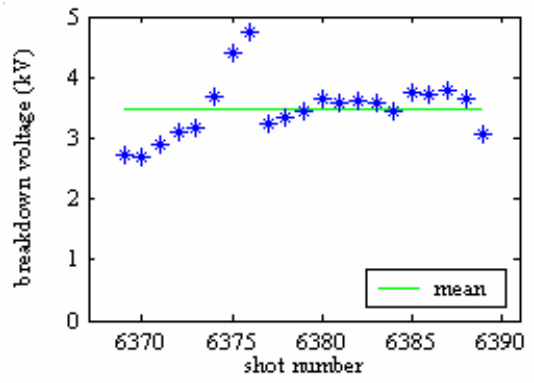

Figure 35. Low energy voltage breakdown test 3 results before a PASD shot.

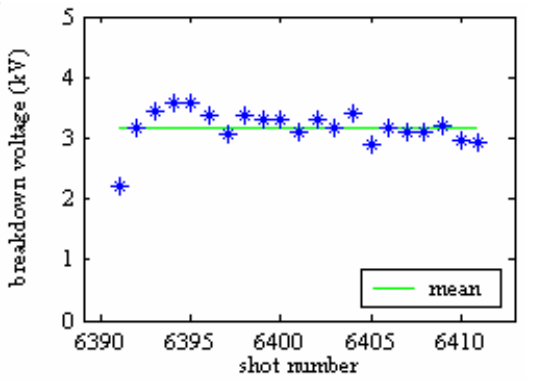

Figure 36. Low energy voltage breakdown test 3 results after a PASD shot.

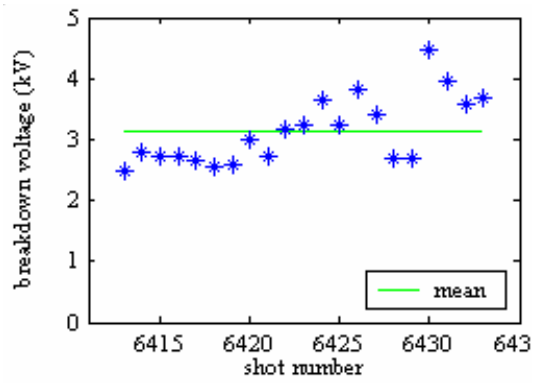

Figure 37. Low energy voltage breakdown test 4 results before a PASD shot.

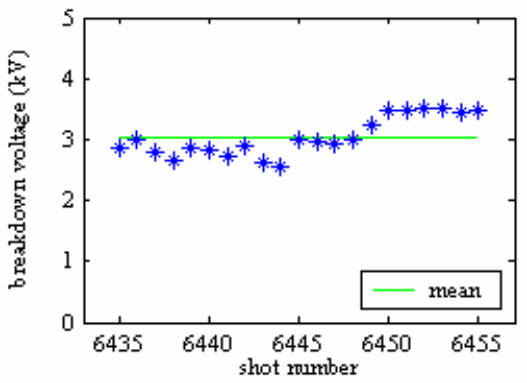

Figure 38. Low energy voltage breakdown test 4 results after a PASD shot.

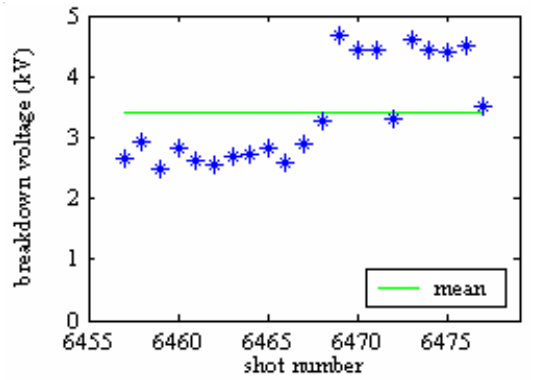

Figure 39. Low energy voltage breakdown test 5 results before a PASD shot.

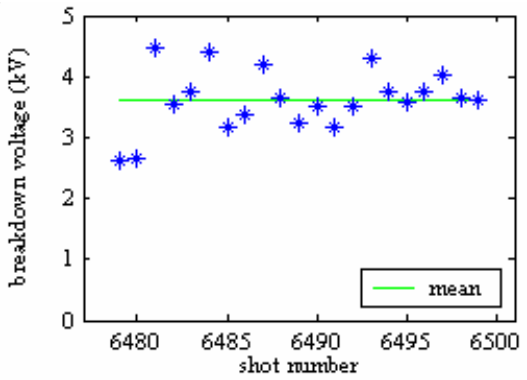

Figure 40. Low energy voltage breakdown test 5 results after a PASD shot.

The data presented in Figure 31 through Figure 40 does not elude to any pattern of change in regard to the average breakdown voltage after the insulator sample is exposed to a PASD pulse. In tests 1, 2, and 5 the average breakdown voltage increases while in tests 3 and 4 the average breakdown voltage decreases. Likewise the maximum deviation from the average in some tests increases after the PASD pulse and in others it decreases. The lack of a consistent change to the breakdown voltage following a PASD pulse is an indication that the PASD pulse does not affect the low energy breakdown voltage.

3.3 Effect of High Energy Discharge on low energy Voltage Breakdown

To investigate the effect of high energy discharge upon the voltage breakdown of the mylar sample the procedure given in section 3.2 is implemented with the PASD experiment listed in step 3 changed to a high energy experiment. The capacitors are charged to ~13kV. In Figure 41 through Figure 50 the results of five different tests are plotted.

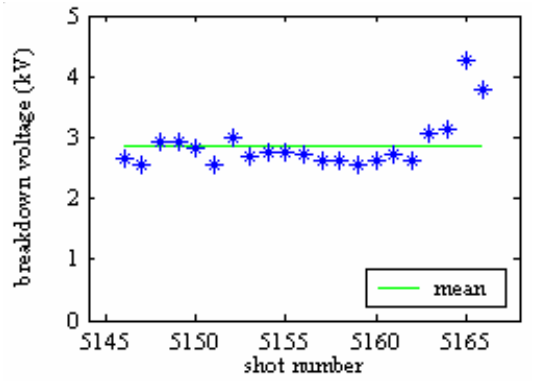

Figure 41. Low energy voltage breakdown test 1 results before a high energy breakdown.

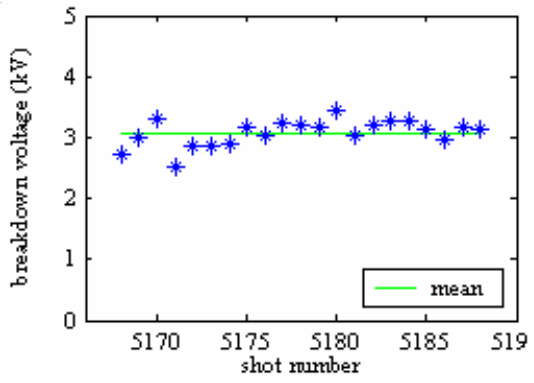

Figure 42. Low energy voltage breakdown test 1 results after a high energy breakdown.

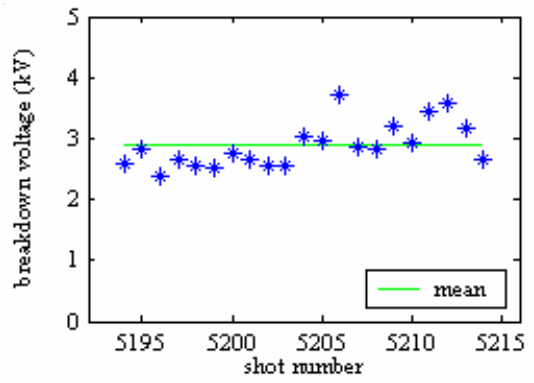

Figure 43. Low energy voltage breakdown test 2 results before a high energy breakdown.

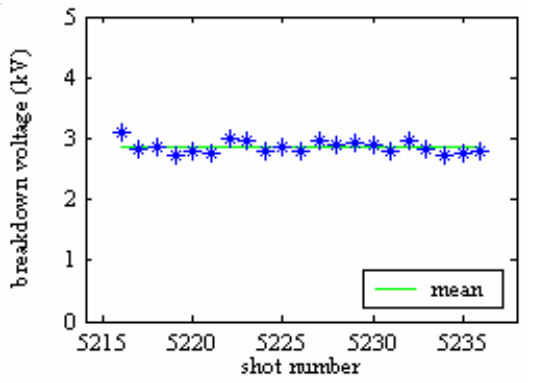

Figure 44. Low energy voltage breakdown test 2 results after a high energy breakdown.

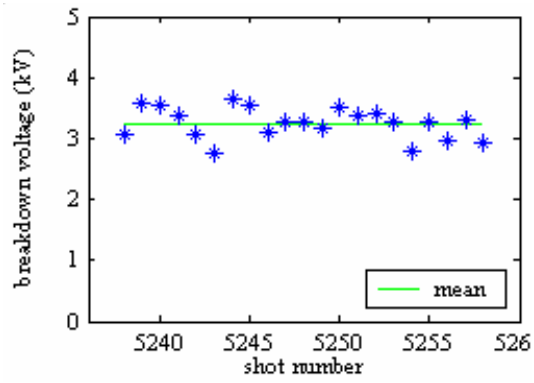

Figure 45. Low energy voltage breakdown test 3 results before a high energy breakdown.

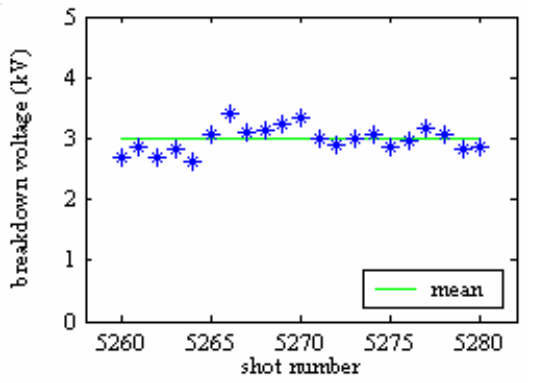

Figure 46. Low energy voltage breakdown test 3 results after a high energy breakdown.

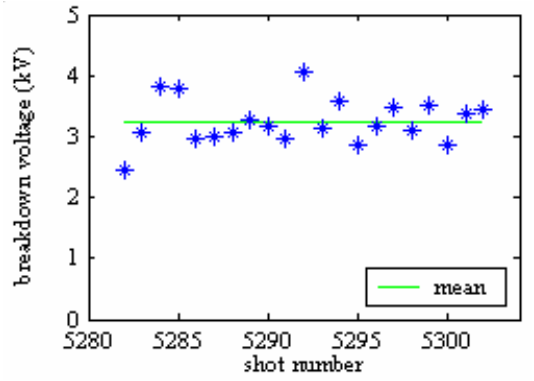

Figure 47. Low energy voltage breakdown test 4 results before a high energy breakdown.

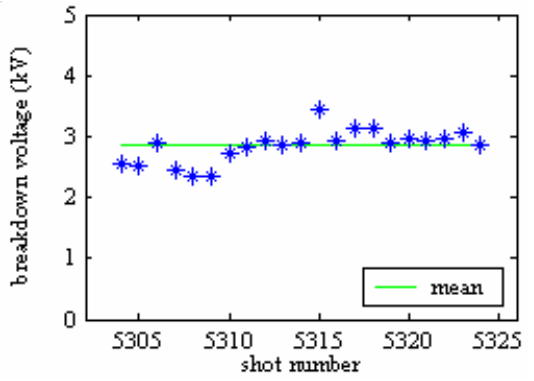

Figure 48. Low energy voltage breakdown test 4 results after a high energy breakdown.

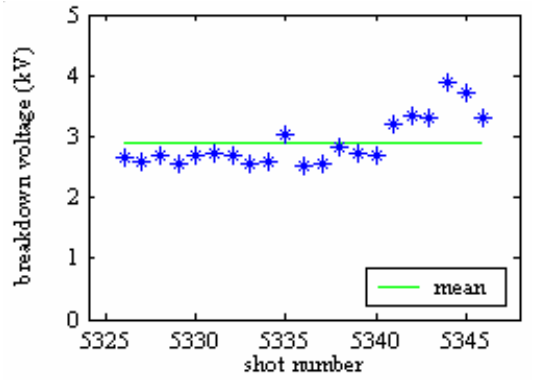

Figure 49. Low energy voltage breakdown test 5 results before a high energy breakdown.

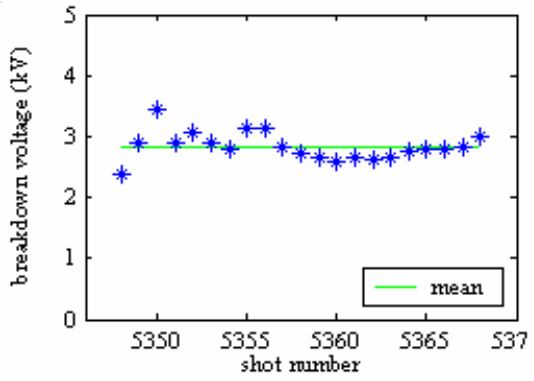

Figure 50. Low energy voltage breakdown test 5 results after a high energy breakdown.

The data presented in Figure 41 through Figure 50 again suggests no pattern of change in regard to the average breakdown voltage after the insulator sample is exposed to a high energy discharge. In tests 2 and 5 the average breakdown voltage stays about the same, in test 1 the average breakdown voltage increases, and in tests 3 and 4 the average breakdown voltage decreases. Unlike the effect of the PASD pulse the spread between the maximum and minimum breakdown voltages either stays about the same or decreases after a high energy pulse occurs across the sample. This apparent trend in the change to breakdown voltage deviation following a high energy discharge may be an indication that the high energy deposition is effecting the insulating material. The next section on microscopic comparisons helps to support the results found in the low energy breakdown tests.

3.4 Microscopic Comparison of Insulator damage

The previous sections on the effects of PASD pulses and high energy discharge on voltage breakdown only found one noticeable trend in the data. That trend is the reduction in the variation of the breakdown voltage following a high energy discharge across a sample. This section supports the trend found in the breakdown voltage following a high energy discharge and the lack of trends following the PASD pulse.

Figure 51 through Figure 56 show photographs of the mylar samples taken before and after discharge tests. The bending and deformation of the samples around the edges are a result of being placed in the test fixture and is independent of the type of voltage breakdown occurring across the samples. This deformation is more easily seen in some photographs than others and is dependent upon the lighting.

Figure 51 and Figure 52 contain photographs of a mylar sample before and after a low energy discharge. Notice the contamination (specs) apparent in Figure 52 following the low energy discharge. Since this contamination is located in areas not in the discharge path they were likely to have been in the fixture prior to the test. The important item to note is the lack of evidence in the photograph of damage to the insulator as a result of the discharge.

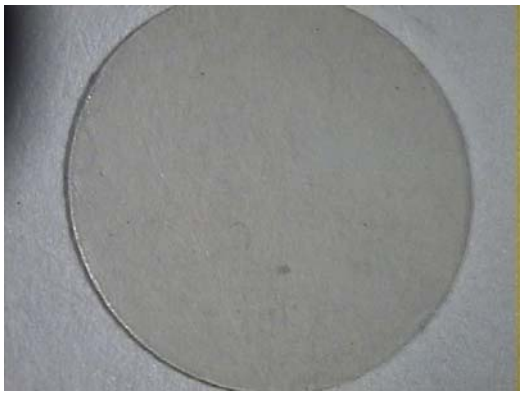

Figure 51. Microscopic photograph of a mylar sample before a low energy breakdown.

Figure 52. Microscopic photograph of a mylar sample after a low energy breakdown.

Figure 53 and Figure 54 contain photographs of a mylar sample before and after a PASD pulse. Notice the contamination (specs) apparent in Figure 54 following the PASD pulse. This contamination is significantly less than the contamination apparent in Figure 52. It is unclear whether the PASD pulse removed some of the contamination or there was less contamination in the fixture during the test. Again the important item to note is the lack of evidence in the photograph of damage to the insulator as a result of the discharge.

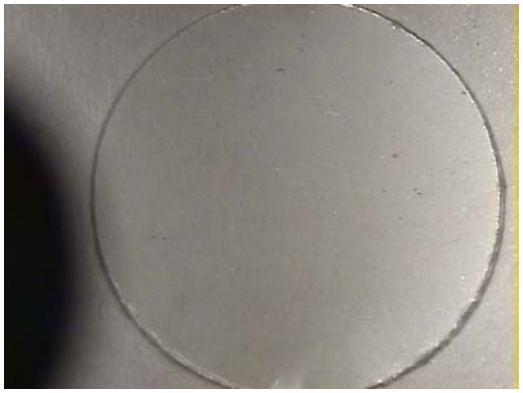

Figure 53. Microscopic photograph of a mylar sample before a PASD pulse.

Figure 54. Microscopic photograph of a mylar sample after a PASD pulse.

Figure 55 and Figure 56 contain photographs of a mylar sample before and after a high energy discharge. Notice the material deposition apparent in Figure 56. This material deposition is suspected to be metal removed from the BNC connector pin depicted in Figure 6. This deterioration is evident by looking at the photograph of this pin in Figure 57. This deposition supports the observation section 3.3 of the high energy discharge affecting the low energy voltage breakdown of the mylar samples.

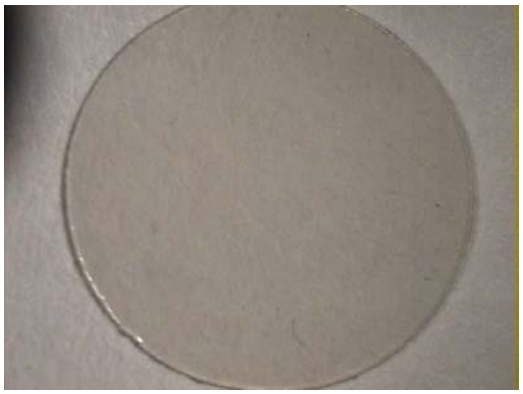

Figure 55. Microscopic photograph of a mylar sample before a high energy discharge.

Figure 56. Microscopic photograph of a mylar sample after a high energy discharge.

4 Conclusions, observations, and suggestions

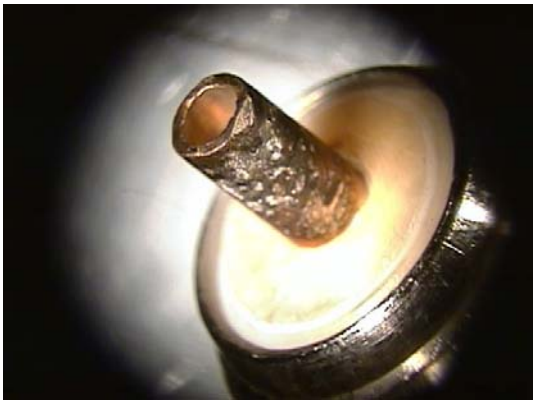

Figure 57. BNC connector pin located in the arc test fixture.

Based on the data presented in this paper, it is believed that the PASD pulse does not damage the insulator under test. In fact, there was no evidence of breakdown strength changes after the first PASD pulse, other than the expected statistical variation, there was no evidence of an effect upon the low energy breakdown voltage after a PASD pulse, and microscopic inspection did not indicate any material deposition. The energy deposition into the arc is dependent on geometry and material, varying from 3.45 mJ to 6.38 mJ. To put the PASD pulse energy level into perspective, consider the energy dissipated during electrostatic shock. For example after a person walks across a carpeted room. Estimating the built up charge voltage to be 25 kV [4](page 72) and a typical value of human body capacitance to be 50pF [4](page 670) the stored energy in the human body is 15.6 mJ. That is three times the energy dissipated by the PASD pulse.

Unlike the PASD pulse, the high energy discharge was found to affect the insulator samples. The variation in the low energy breakdown voltage was observed to decrease and material deposition was visible when viewed under a microscopic.

The logical next steps, given the inability to detect damage resulting from the PASD pulse, are to investigate the capabilities of the PASD diagnostic to detect defects in aircraft wiring systems and to develop a prototype portable pulser. However, some further experiments to prove the non-destructive nature of PASD may be warranted.

4.1 Recommended future tests

The goal of establishing an energy threshold at which damage to the insulator can be detected was not achieved. Even experiments at one hundred times the PASD pulse energy failed to decrease the insulation strength of the sample under test. Repeating these experiments at higher energy levels may be possible, but other effects may begin to dominate the breakdown process and complicate the analysis. Higher energy levels are likely to remove metal from the test fixture electrodes that would then containment the sample. This effect would be very dependent on the geometry and materials used for the anode and cathode and may not shed meaningful light on how PASD would perform in aircraft wiring systems. The fact that the breakdown strength of the insulators tested in this report were not altered by energy deposition one hundred times the anticipated PASD pulse energy strongly suggests that PASD is entirely non-destructive. However, we may want to test additional insulation materials, including those used in typical aircraft connectors.

Additionally, since an understanding of the source of the specks of contamination seen in Figure 52, Figure 54, and Figure 56 is not known, further tests involving before and after photographs are recommended in order to determine any patterns and the probable source.

The focus of this test report was strictly the effect of PASD on surface properties of insulating materials. This analysis is relevant to situations where the insulation has been breached all the way through to the conductor as shown in Figure 58.

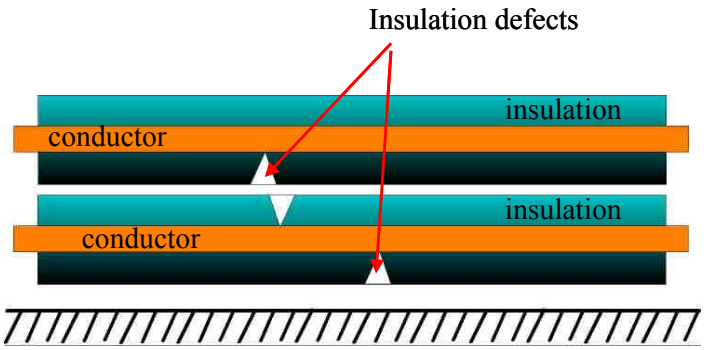

Figure 58. Insulator breached to the conductor.

There could be a situation where some small degree of insulation is left on a conductor (see Figure 59) and application of the PASD pulse may produce an insulation failure. Punching through this small amount of insulation would then very likely affect the breakdown strength of the insulator if tested after the PASD pulse. However, it could also be argued that it would be beneficial if PASD did punch through the small layer of remaining insulation. The benefit would be the identification of the insulation defect. Data on this scenario could be collected in year two of the PASD development program.

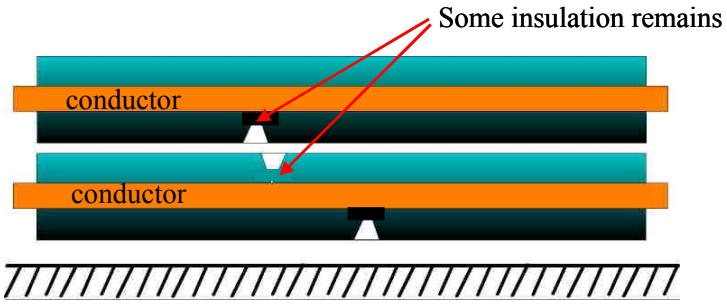

Figure 59. Insulator damaged but not breached to the conductor.

5 References

[1] Dinallo and Schneider,'Pulsed Arrested Spark Discharge (PASD Diagnostic Technique for the Location of Defects in Aging Wiring', SAND2001-3225

[2] R.J.Smith, "Circuits, Devices, and Systems", John Wiley and Sons, 1967

[3] Ramo, Whinnery, and Van Duzer "Fields and Waves in Communication Electronics', John Wiley and Sons, 1965

[4] C.R.Paul, "Introduction to Electromagnetic Compatibility," John Wiley and Sons, Inc. 1992

Distribution

1	MS	9018	Central Technical Files, 8945-1
2		0899	Technical Library, 9616
4	MS	1152	Larry Schneider, 1643
2		1152	Steven Glover, 1643
1		1152	Matthew Higgins, 1643
1		1152	Gary Pena, 1643
1		1152	Mike Dinallo, 1643
10		1182	Tom Lockner, 15335
4			Robert Pappas, AAR-480 William J. Hughes Tech. Center Atlantic City International Airport Atlantic City, NJ 08405